

Mode-II fracture behaviour of aerospace-grade carbon fibre/epoxy composites interleaved with thermoplastic veils

Quan, Dong; Bologna, Francesca; Scarselli, Gennaro; Ivanković, Alojz; Murphy, Neal

DOI

[10.1016/j.compscitech.2020.108065](https://doi.org/10.1016/j.compscitech.2020.108065)

Publication date

2020

Document Version

Accepted author manuscript

Published in

Composites Science and Technology

Citation (APA)

Quan, D., Bologna, F., Scarselli, G., Ivanković, A., & Murphy, N. (2020). Mode-II fracture behaviour of aerospace-grade carbon fibre/epoxy composites interleaved with thermoplastic veils. *Composites Science and Technology*, 191, Article 108065. <https://doi.org/10.1016/j.compscitech.2020.108065>

Important note

To cite this publication, please use the final published version (if applicable).
Please check the document version above.

Copyright

Other than for strictly personal use, it is not permitted to download, forward or distribute the text or part of it, without the consent of the author(s) and/or copyright holder(s), unless the work is under an open content license such as Creative Commons.

Takedown policy

Please contact us and provide details if you believe this document breaches copyrights.
We will remove access to the work immediately and investigate your claim.

Mode-II fracture behaviour of aerospace-grade carbon fibre/epoxy composites interleaved with thermoplastic veils

Dong Quan^a, Francesca Bologna^b, Gennaro Scarselli^{b,c}, Alojz Ivanković^b, Neal Murphy^{b,*}

^a*Structural Integrity & Composites Group, Faculty of Aerospace Engineering, Delft University of Technology, Netherlands*

^b*School of Mechanical and Materials Engineering, University College Dublin, Ireland*

^c*Department of Innovation Engineering, University of Salento, Italy*

Abstract

Thermoplastic veils based on Polyethylene-terephthalate (PET), Polyphenylene-sulfide (PPS) and Polyamide-12 (PA) fibres ($\sim 10\ \mu\text{m}$ in diameter) were used to interlay unidirectional (UD), non-crimp fabric (NCF) and 5-Harness satin weave (5H) carbon fibre laminates. The PET and PPS veils remained in a fibrous form and the PA veils melted during the laminate curing process. The results of an end-loaded split test demonstrated significant improvements in the mode-II fracture performance in all cases. In general, interlaying thermoplastic veils was most efficient for toughening the UD laminates, with reduced improvements observed for the 5H and NCF laminates, respectively. The main toughening mechanism of the intact PET and PPS veils was thermoplastic fibre bridging. The melted PA veils mainly improved the fracture toughness of the epoxy at the mid-plane. The different toughening mechanisms of the veils, combined with different fracture mechanisms between the UD, NCF and 5H laminates, resulted in significantly different toughening levels.

Keywords: A: Polymer-matrix composites (PMCs); Thermoplastic veils; B: Fracture toughness; C: Fibre bridging; D: Fractography.

*Corresponding author. Tel: +353 (1) 7161940; Email: neal.murphy@ucd.ie (Neal Murphy)

1. Introduction

The poor interlaminar fracture toughness of fibre reinforced plastics (FRPs) resulting from their laminated structure is a major constraint on their wider use. A number of methods have been developed to improve the interlaminar fracture toughness of FRPs, among which, the following three strategies are most prevalent: (1) incorporating second phase modifiers to the epoxy matrix, such as silica-rubber hybrid nanoparticles [1], carbon nanotubes [2], and nano-clay [3]; (2) changing the architecture of the fibre mats using various techniques, i.e. 3D textile weaving [4], Z-pinning [5] and stitching [6]; and (3) interlaying the FRPs using various materials, including carbon fibres [7], carbon nanomaterials [8], stainless steel fibres [9], thermoplastic films [10] and thermoplastic veils [11]. Various levels of success have been achieved based on different strategies. However, there are shortcomings associated with these techniques, such as: the incorporation of second phase modifiers (strategy 1) typically increases the viscosity of the matrix, resulting in significant processing challenges; changing the architecture (strategy 2) of fibre mats using 3D textile weaving, Z-pinning and stitching can lead to a considerable drop in the in-plane properties [6, 12, 13]; interlaying materials, such as stainless steel fibres [9], can result in an increase in the composite weight; and adding thermoplastic film interlayers can hinder the resin impregnation during the transfer moulding of the laminates.

The tough, ductile, porous and lightweight nature of thermoplastic veils based on either nano-/micro-scale fibres, makes them an attractive option for interlaying FRPs. For example, their porous architecture will not hinder resin impregnation during the manufacturing process of FRPs [14]. This porous architecture, together with a high specific surface area of the micro- or nano- thermoplastic fibres, can considerably promote the bonding to the matrix phase. It is generally accepted that interlaying thermoplastic veils can considerably enhance the interlaminar toughness of the FRPs [11, 15–21]. Moreover, a number of studies demonstrated that interlaying thermoplastic veils into FRPs had no detrimental effects on the other mechanical properties, such as flexural modulus and strength [15, 22–24], and interlaminar

shear strength [15–17, 23]. For these reasons, interlaying thermoplastic veils in FRPs is attracting the attention of both researchers and industrialists [21]. Notwithstanding, adverse effects on the fracture responses of FRPs upon interlaying thermoplastic veils were also reported by some other literature [14, 24–26]. The toughening performance of the thermoplastic veils can be affected by many factors, including the areal density of the veils [14–16, 27, 28], the veil material [14, 19, 26, 29], the form of the veils in the FRPs, i.e. melted or non-melted [19, 22, 30] and the architecture of the carbon fibre fabrics [20, 26, 28, 29]. To date, no conclusive effects of these factors can be drawn based on the limited number of studies, as in which, different FRP systems and material types and areal densities of thermoplastic veils were used. Moreover, the effects of interlaying thermoplastic veils on the fracture response of CFRPs specifically for aerospace applications have received very little attention.

The aim and main novelty of this work are to comprehensively investigate the effects of interlaying thermoplastic veils on the mode-II fracture performance of commercialised aerospace-grade CFRPs. Thermoplastic veils with various areal densities based on Polyethylene-terephthalate (PET), PPS and Polyamide-12 (PA) fibres ($\sim 10 \mu\text{m}$ in diameter) were used to reinforce three types of aerospace-grade CFRPs manufactured from unidirectional (UD) prepregs, 5-Harness weave (5H) prepregs, and resin transfer moulding (RTM) of non-crimp carbon fibre fabric (NCF). The PET and PPS veils remained in a fibrous form, and the PA veils melted during the laminate curing cycle. The mode-II fracture behaviour and corresponding toughening mechanisms of the interleaved laminates were systematically studied.

2. Experimental

2.1. Materials

Three types of CFRPs based on unidirectional carbon fibre fabrics (UD), non-crimp carbon fibre fabrics (NCF) and 5-Harness satin weave carbon fibre fabrics (5H) were used in this work. The UD and 5H prepregs were HYE-1034E from Cytac (Solvay Group, UK), and Hexply 8552/5H from Hexcel (UK), respectively. They possessed an areal density of

230 g/m² and 615 g/m², respectively, and a fibre volume fraction of 57-63 % and 55 %, respectively. The dry non-crimp carbon fibre fabrics (NCF), with an areal density of 575 g/m², were biaxial Toray T700Sc 50C from Saertex GmbH (Germany). The epoxy resin for resin transfer moulding (RTM) of the NCF laminates was CYCOM 890RTM from Cytec (Solvay Group, UK). The NCF laminates had a fibre volume fraction of 55 %. The thermoplastic veils based on Polyethylene-terephthalate (PET), Polyphenylene-sulfide (PPS) and Polyamide-12 (PA) were supplied by Technical Fibre Products Ltd. (UK). The average diameters of the PET, PPS and PA fibres were $13.2 \pm 2.3 \mu\text{m}$, $9.5 \pm 1.1 \mu\text{m}$ and $11.7 \pm 1.5 \mu\text{m}$, respectively [31]. In this paper, the thermoplastic veils will be referred to as the polymer type followed by its areal density, e.g. PPS10 represents a 10 g/m² PPS veil.

2.2. *Manufacture and Characterisation of the CFRPs*

For the UD and 5H laminates, a layup consisting of 26 plies of UD prepregs or 14 plies of 5H prepregs was firstly placed under vacuum for 45 mins to remove air pockets and to consolidate the layup. For the NCF laminates, a [90, 0]_s-layup was impregnated by the epoxy resin using a vacuum-assisted RTM process, during which the resin was heated up to 80 °C to reduce its viscosity. A layer of thermoplastic veil was placed at the mid-plane of the laminates during the layup process to prepare interleaved CFRPs. The same curing schedule was then used to cure all the laminate layups in an in-house pressclave. The laminate was cured inside an aluminium mould under vacuum with an internal pressure of 0.5 MPa in the mould chamber. The cure cycle consists of a 2-hour ramp from room temperature to 180 °C followed by a 2-hour hold, or dwell, at 180 °C. To avoid post-curing warping, the laminate was kept in the pressclave under full pressure and vacuum until the temperature cooled down naturally to 80 °C. The composite laminate was then taken out of the mould after the temperature dropped to room temperature, and cut into the required dimensions for the subsequent tests. The crack starter of the samples for fracture tests was generated by placing a PTFE insert (with a thickness of 12.5 μm) at the mid-plane. It should be noted that the melting temperatures of the PET, PPS and PA veils were measured to be 250 °C, 290 °C

and 180 °C, respectively [31]. Hence, the PET and PPS veils remained in their fibrous form, and the PA veils melted during the hot-curing process at 180 °C.

An end-loaded split (ELS) test was carried out to study the mode-II fracture behaviour of the CFRPs according to ISO:15114 [32]. The flexural moduli of the UD, NCF and 5H laminates were measured to be 131.0 GPa, 59.9 GPa and 64.5 GPa, respectively, using a clamp calibration test described in ISO:15114. The ELS tests were conducted at a constant displacement rate of 1 mm/min on specimens having a length of 190 mm and a width of 20 mm. Before the test, a sharp precrack was firstly generated under mode-I opening load. The crack length was recorded at 1 mm increments for the first 10 mm and then at 2.5 mm increments for the rest of the test using a travelling digital microscope. The mode-II fracture energy was calculated based on the corrected beam theory [32]. At least three replicate tests were conducted for each set. The fracture surfaces of the specimens were then gold sputtered for 20 s, and imaged using a scanning electron microscope (TM4000 from Hitachi).

3. Results and Discussion

3.1. Mode-II fracture of the CFRPs with no thermoplastic veils

Figure 1 shows R -curves from the ELS tests of the UD, NCF and 5H controls. Three

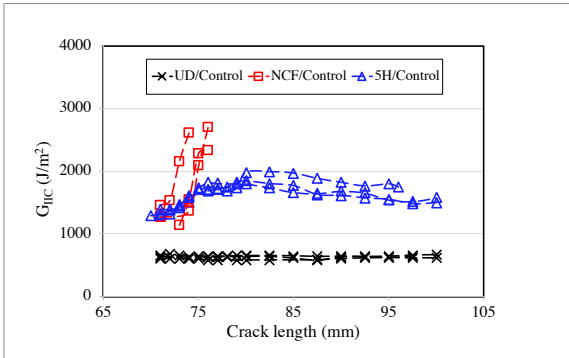


Figure 1: Representative R -curves from the ELS tests of the control laminates.

typical types of R -curves from the ELS tests were observed: (I) the R -curves remained reasonably ‘flat’ (UD/Control); (II) the R -curves initially rose and then plateaued (5H/Control); and (III) the R -curves followed an upward trend (NCF/Control). These R -curve behaviours were representative for all the specimens in this study. Herein, to calculate the mode-II fracture energy, $G_{IIC}^{plateau}$ was taken as the average of all the values at the plateau region of the ‘rising-plateau’ R -curves, and G_{IIC}^{max} was taken as the maximum values of the ‘rising’ R -curves. Both $G_{IIC}^{plateau}$ and G_{IIC}^{max} were taken as the fracture propagation energy (G_{IIC}^{prop}) for each case. It should be noted that some R -curves, especially for the NCF and 5H laminates, exhibited a rather complex trend, such as slightly decreasing or highly scattered, after an initial rising stage. This was the result of a local non-uniformity in the structures of the specimens. They were also classified as conforming to ‘rising-plateau’ R -curves in this paper. As recommended in [32], a 5% offset approach was used to determine the crack initiation energy (G_{IIC}^{ini}) for all the UD and 5H laminates. However, this approach led to unrealistically high values for G_{IIC}^{ini} of the NCF laminates. Hence, a non-linear point approach [32] was used to determine G_{IIC}^{ini} of the NCF laminates. It should be noted that, in general, G_{IIC} values were calculated and reported for a crack length range of 70-100 mm. If the R -curve terminated for crack lengths shorter than 100 mm, it means that the specimen failed dynamically at the last point.

Significantly different fracture behaviours were observed for different control laminates, as shown in Figure 1, i.e. the type of R -curve was ‘flat’ for the UD/Control, ‘rising’ for the NCF/Control and ‘rising-plateau’ for the 5H/Control. Additionally, the crack stably propagated through the entire ELS testing region for the UD and 5H controls. The NCF/Control failed dynamically (the crack suddenly jumped to the end of the specimens) after the crack propagated a few millimetres. The values of the fracture energy for the control laminates are summarised in Table 1. It was found that the NCF/Control possessed the highest fracture energy, followed by the 5H/Control, and then the UD/Control. For example, the fracture propagation energy was measured to be 2549 J/m², 1721 J/m² and 627 J/m² for the NCF, 5H

Specimens	G_{IIC}^{ini} (J/m ²)	$G_{IIC}^{plateau}$ (J/m ²)	G_{IIC}^{max} (J/m ²)
UD/Control	630±26	627±22	*
NCF/Control	1185±115	*	2549±192
5H/Control	1340±41	1721±132	*

and UD controls, respectively.

3.2. Unidirectional (UD) CFRPs interleaved with thermoplastic veils

The R -curves of the UD laminates interleaved with different thermoplastic veils are shown in Figure 2, and the corresponding fracture energies are presented in Table 2. It was

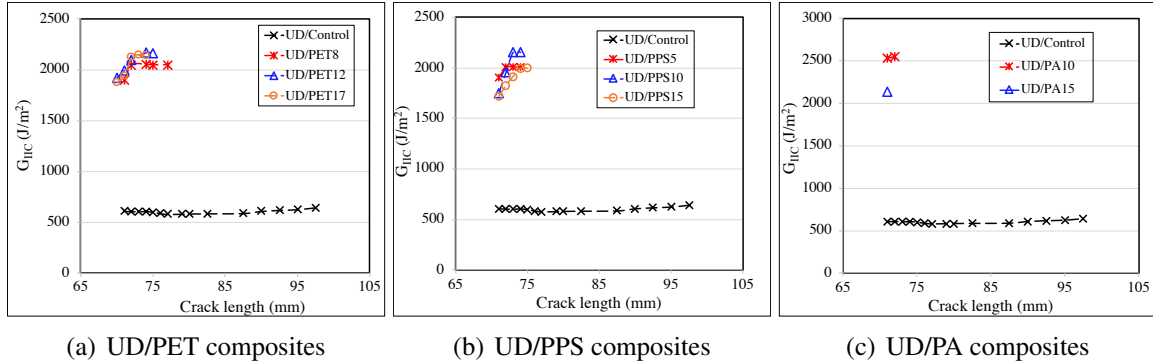


Figure 2: Representative R -curves of the UD laminates interleaved with thermoplastic veils.

observed that interlaying thermoplastic veils resulted in an alteration of the crack growth characteristics from stable propagation for the UD control to dynamic propagation for all the interleaved UD laminates, see Figure 2. For example, dynamic fracture of the entire specimen took place for the laminates interleaved with the PA veils, referring to only one or two points on the corresponding R -curves in Figure 2 (c). Significant improvements in the fracture energy were obtained for all the interleaved UD laminates, as shown in Table 2. A value of 630 J/m² was measured for G_{IIC}^{ini} of the UD/Control. The maximum values of G_{IIC}^{ini} were measured to be 1868 J/m² (UD/PET12), 1807 J/m² (UD/PPS15) and 2520 J/m² (UD/PA10) for the UD laminates interleaved with PET, PPS and PA veils, respectively. This corresponds

Table 2: G_{IIC} of the interleaved UD laminates. Values in brackets indicate percentage increase of G_{IIC}^{ini} values over those of control specimens.

Specimens	G_{IIC}^{ini} (J/m ²)	$G_{IIC}^{plateau}$ (J/m ²)	G_{IIC}^{max} (J/m ²)
UD/Control	630±26	627±22	*
UD/PET8	1691±21 (+168 %)	*	1968±72
UD/PET12	1868±103 (+197 %)	*	2051±103
UD/PET17	1768±60 (+181 %)	*	1982±143
UD/PPS5	1654±178 (+163 %)	*	1939±101
UD/PPS10	1783±46 (+183 %)	*	2128±57
UD/PPS15	1807±228 (+187 %)	*	2053±77
UD/PA10	2520±303 (+300 %)	*	2697±117
UD/PA15	2042±104 (+224 %)	*	2096±80

to an increase of 197 %, 187 % and 300 %, respectively. Similarly, the mode-II fracture propagation energy significantly increased from 627 J/m² ($G_{IIC}^{plateau}$) for the UD/Control to 2051 J/m² (G_{IIC}^{max}) and 2128 J/m² (G_{IIC}^{max}) for the PET and PPS interleaved UD laminates, and further to 2697 J/m² (G_{IIC}^{max}) for the PA10 interleaved laminates. Representative pictures and microscopy images of the fracture surfaces of the ELS specimens for the interleaved UD laminates are shown in Figure 3. The yellow dashed boxes indicate the stable crack propagation region. It is clear that the addition of thermoplastic veils decreased the length of the stable crack propagation region in all cases. This corresponds to the dynamic failure of the interleaved laminates, as observed in Figure 2. Typical smooth fracture surfaces without any sign of carbon fibre bridging were observed for the UD/Control laminate. The majority of the thermoplastic fibres remained on the upper fracture surface for the PET and PPS veil interleaved UD laminates, see Figure 3. This demonstrated an interfacial failure between the carbon fibres and the thermoplastic veils dominating the fracture. In this case, no additional thermoplastic fibres were involved in the fracture as the areal density of the veils increased, and hence, the areal density of the veils had a negligible effect on the fracture energy for

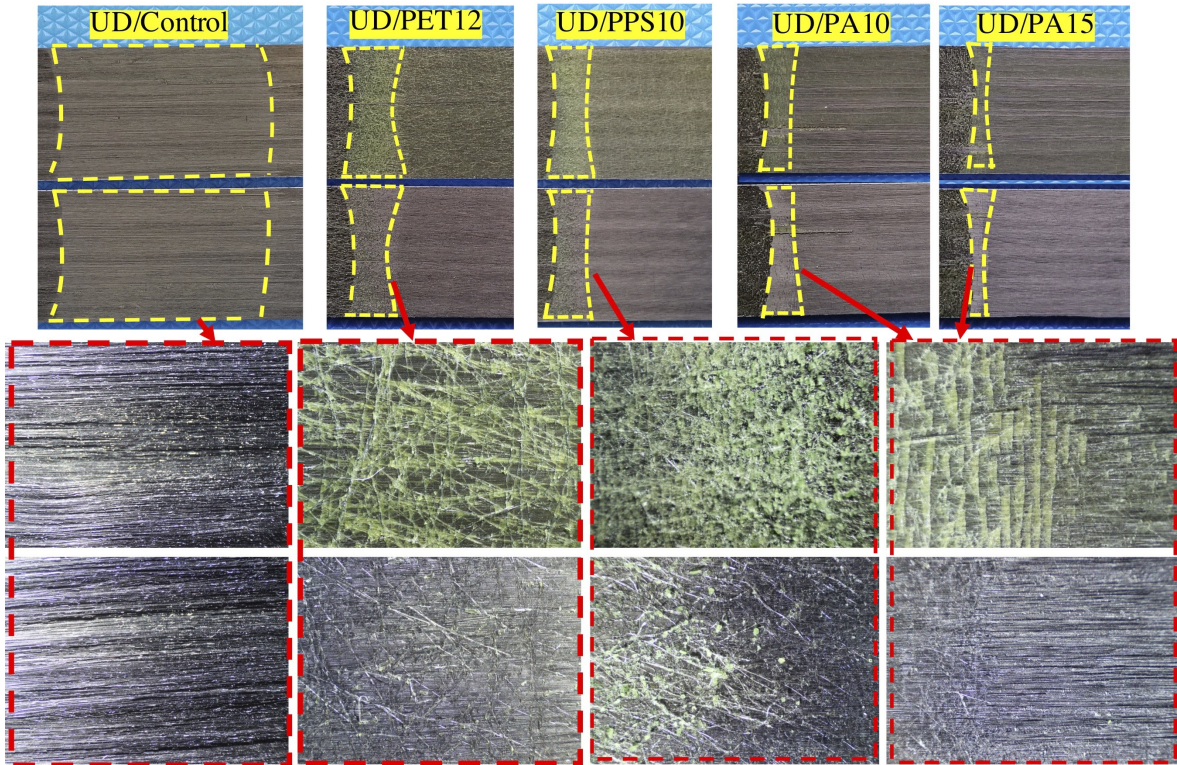


Figure 3: Representative photographs (top) and light microscopy images (bottom) of the fracture surfaces of the UD laminates. The yellow dashed boxes indicate the stable crack propagation region. The light microscopy images were taken from within the boxes.

the PET and PPS interleaved UD laminates, see Table 2. An interfacial failure between the carbon fibre tows and the toughened PA/epoxy layer also took place for the PA interleaved UD laminates, see Figure 3. However, interlaying PA veils led to an extremely unstable fracture behaviour of the UD laminates, evidenced by the short crack propagation region for the PA interleaved UD laminates in Figure 3. Increasing the areal density of the PA veils from 10 g/m² to 15 g/m² caused a significant decrease in the length of the stable crack propagation region. This phenomenon was associated with a drop in the length of the fracture process zone ahead of the crack tip during the fracture process, and subsequently led to a decrease in the fracture energy, as shown in Table 2.

3.3. Non-crimp fabric (NCF) CFRPs interleaved with thermoplastic veils

Figure 4 shows the *R*-curves of the NCF laminates interleaved by different thermoplastic veils, and Table 3 summarises the corresponding fracture energies. The incorporation of the

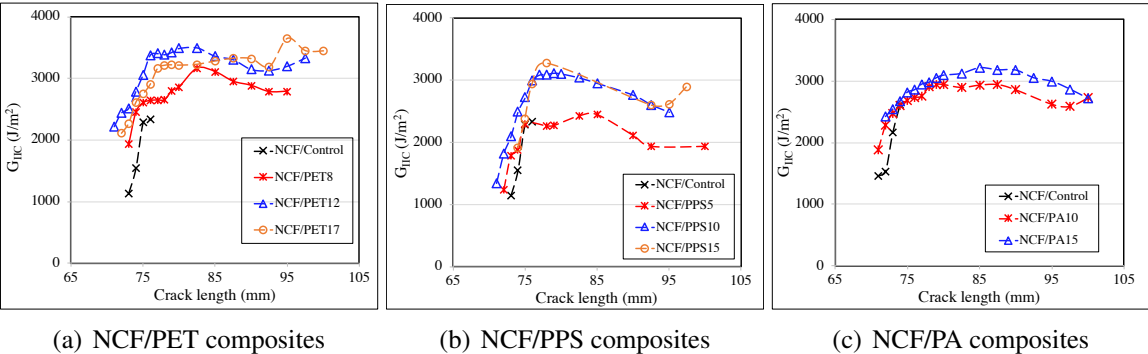


Figure 4: Representative *R*-curves of the NCF laminates interleaved with thermoplastic veils.

thermoplastic veils changed the crack growth behaviour from a dynamic failure for the NCF control (which took place at a crack length of 76 mm for the given example) to a stable failure for all the interleaved laminates, see Figure 4 . In general, noticeable improvements in both G_{IIC}^{ini} and G_{IIC}^{prop} ($G_{IIC}^{plateau}$ or G_{IIC}^{max}) of the NCF laminates were obtained by interlaying the thermoplastic veils, e.g. the maximum value of G_{IIC}^{ini} increased by 64 %, 62 % and 55 % upon interlaying the PET, PPS and PA veils, respectively. Unlike the interleaved UD laminates, the

Table 3: G_{IIC} of the interleaved NCF composites. Values in brackets indicate percentage increase of G_{IIC}^{ini} values over those of control specimens.

Specimens	G_{IIC}^{ini} (J/m ²)	$G_{IIC}^{plateau}$ (J/m ²)	G_{IIC}^{max} (J/m ²)
NCF/Control	1185±115	*	2549±192
NCF/PET8	1804±70 (+52 %)	2914±79	*
NCF/PET12	1929±138 (+63 %)	3510±246	*
NCF/PET17	1938±45 (+64 %)	3332±76	*
NCF/PPS5	1280±129 (+8 %)	2277±150	*
NCF/PPS10	1608±150 (+36 %)	2724±72	*
NCF/PPS15	1925±130 (+62 %)	2908±142	*
NCF/PA10	1736±131 (+46 %)	2791±118	*
NCF/PA15	1832±141 (+55 %)	3163±115	*

areal density of the thermoplastic veils exhibited clear effects on the fracture energy of the PET and PPS interleaved NCF laminates. This was attributed to a cohesive failure inside the thermoplastic veils, as shown in Figure 5, where both the upper and lower fracture surfaces of the NCF/PET12 and NCF/PPS10 specimens were covered with a layer of resin containing thermoplastic fibres. As such, more thermoplastic fibres were involved in the fracture for the NCF laminates interleaved by a veil with a higher areal density. For the NCF laminates with PA veils, the incorporation of melted PA veils enhanced the fracture toughness of the epoxy matrix, and subsequently resulted in significantly additional carbon fibre delamination and bridging. This is indicated by the presence of many delaminated and broken carbon fibres on the fracture surfaces of the NCF/PA10 laminate in Figure 5. These phenomenon contributed to the toughness improvement of the PA interleaved NCF laminates.

3.4. 5-harness satin weave CFRPs interleaved with thermoplastic veils

The R -curves of the 5H laminates interleaved with thermoplastic veils are shown in Figure 6, and the corresponding fracture energies are summarised in Table 4. It was found that the crack stably propagated to a crack length of around 80-90 mm, then dynamically failed

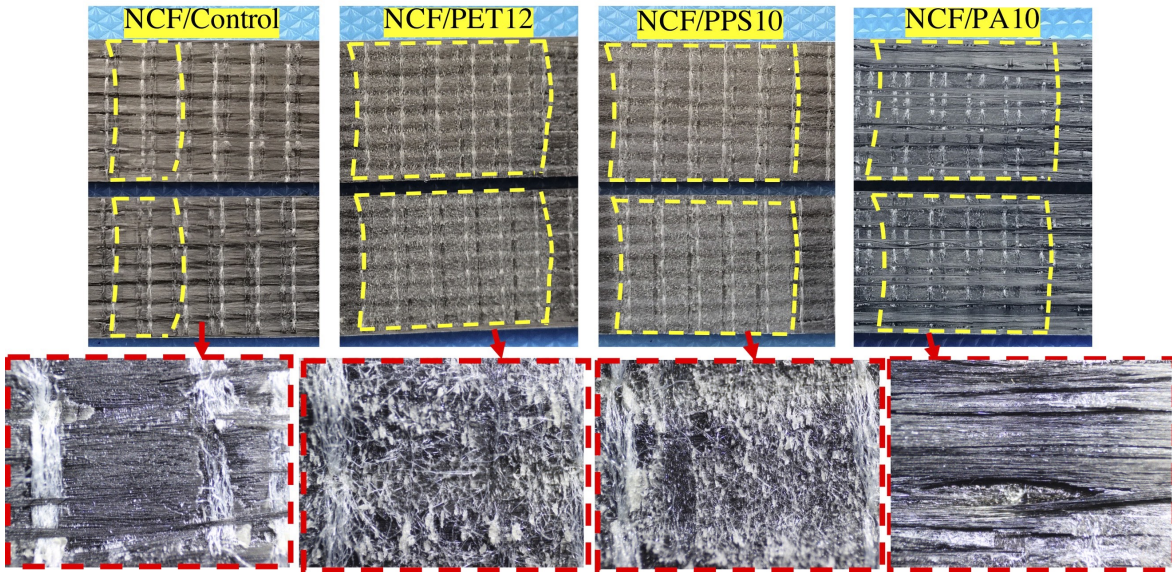


Figure 5: Representative photographs (top) and light microscopy images (bottom) of the fracture surfaces of the NCF laminates. The yellow dashed boxes indicate the stable crack propagation region. The light microscopy images were taken from within the boxes.

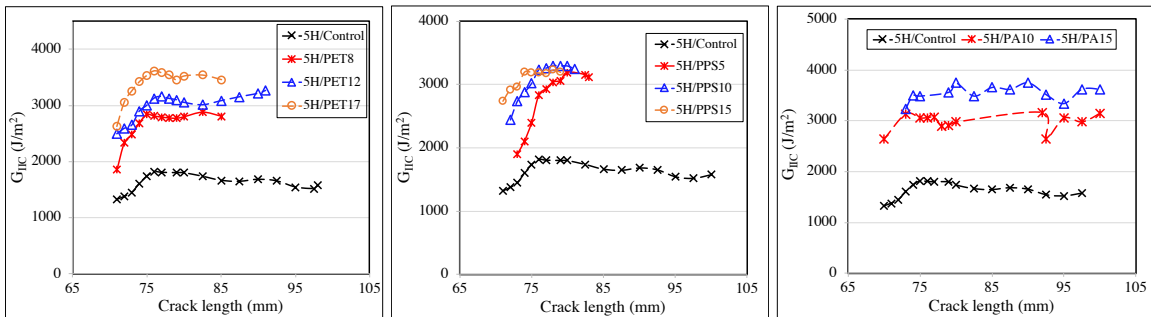


Figure 6: Representative R -curves of the 5H laminates interleaved with thermoplastic veils.

along the entire length of the specimens due to the addition of the non-meltable PET and PPS veils to the 5H laminates. In contrast, interlaying the meltable PA veils had no effect on the stable crack propagation behaviour of the 5H laminates. As expected, interlaying thermoplastic veils significantly improved the fracture energy of the 5H laminates in all cases. G_{IIC}^{ini} was measured to be 1340 J/m² for the 5H/Control. A maximum value of 2459 J/m² (5H/PET17), 2510 J/m² (5H/PPS15) and 3393 J/m² (5H/PA10) were obtained for the 5H laminates interleaved with the PET, PPS and PA veils, respectively. This corresponds to an increase of 84 %, 87 % and 153 %, respectively. Similarly, $G_{IIC}^{plateau}$ was also increased by a maximum of 98 % (5H/PET17), 88 % (5H/PPS15) and 115 % (5H/PA15), respectively. Figure 7 presents representative pictures and microscopy images of the fracture surfaces of the ELS specimens for the interleaved 5H laminates. As before, the yellow dashed boxes indicate the stable crack propagation region. Evidence of carbon fibre bridging, i.e. the presence of delaminated and broken carbon fibres on the fracture surfaces, was observed for the 5H/Control laminates. This explained why the 5H/Control laminate possessed a relatively high fracture energy, when compared to the UD and NCF control laminates, as reported in Section 3.1. The majority of the thermoplastic fibres remained on the upper fracture surfaces for the PET and PPS veil interleaved 5H laminates, see Figure 7. Hence, as in the case of the UD laminates, the fracture mainly took place between the veils and the carbon fibres. This explains why the areal density of the PET and PPS veils had no significant effects on $G_{IIC}^{plateau}$ of the 5H laminates, see Table 4. Moreover, some delaminated carbon fibres appeared on the upper surfaces of the 5H/PET12 and 5H/PPS10 laminates, indicating the existence of carbon fibre bridging during the fracture process. For the 5H/PA10 laminate, the entire layer of the PA resin toughened epoxy was left on the upper fracture surface, leaving only bare carbon fibres on the lower fracture surface, as shown in Figure 7. Additionally, there were extensive carbon fibres attached to the surface of the PA resin, referring to the black colour strips and squares on the upper fracture surfaces of the 5H/PA10 specimen (the numbered locations on the photo for the 5H/PA10 in Figure 7). Hence, a mixture of interfacial failure (between the toughened

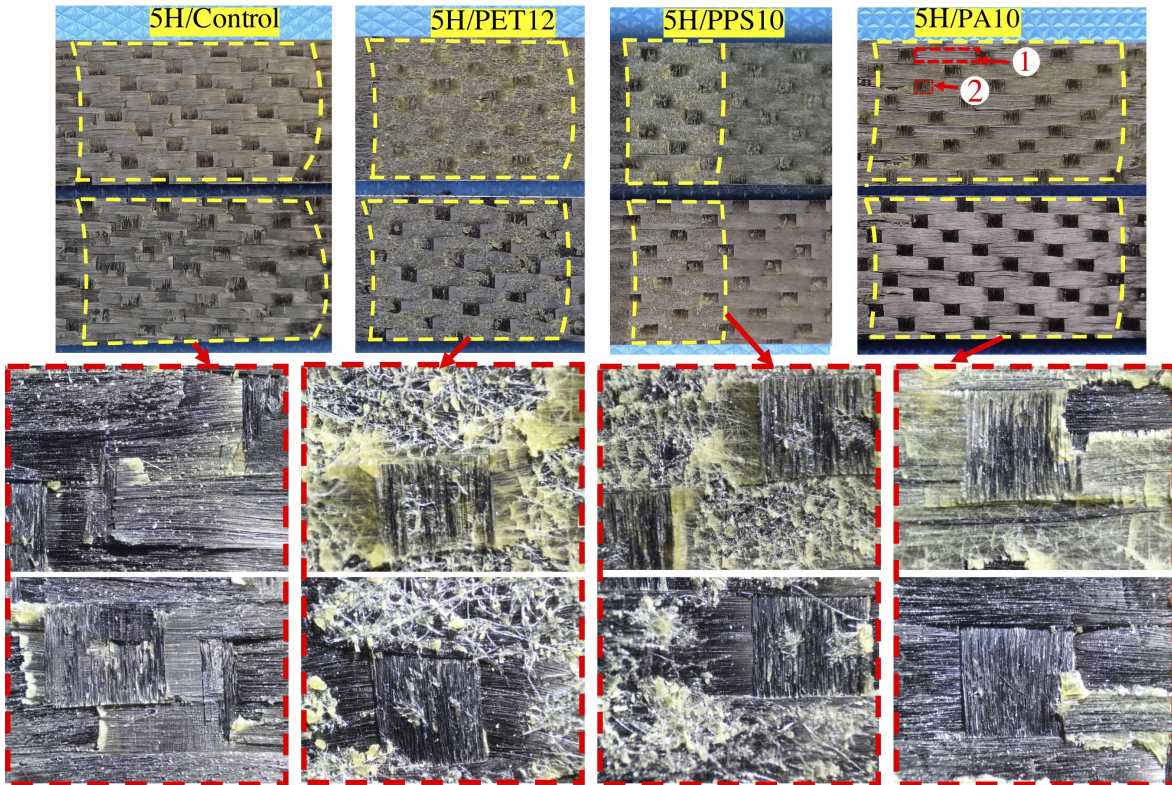


Figure 7: Representative photographs (top) and light microscopy images (bottom) of the fracture surfaces of the 5H laminates. The yellow dashed boxes indicate the stable crack propagation region. The light microscopy images were taken from within the boxes. The numbers in the figures for 5H/PA10 refer to strips of delaminated and broken carbon fibres.

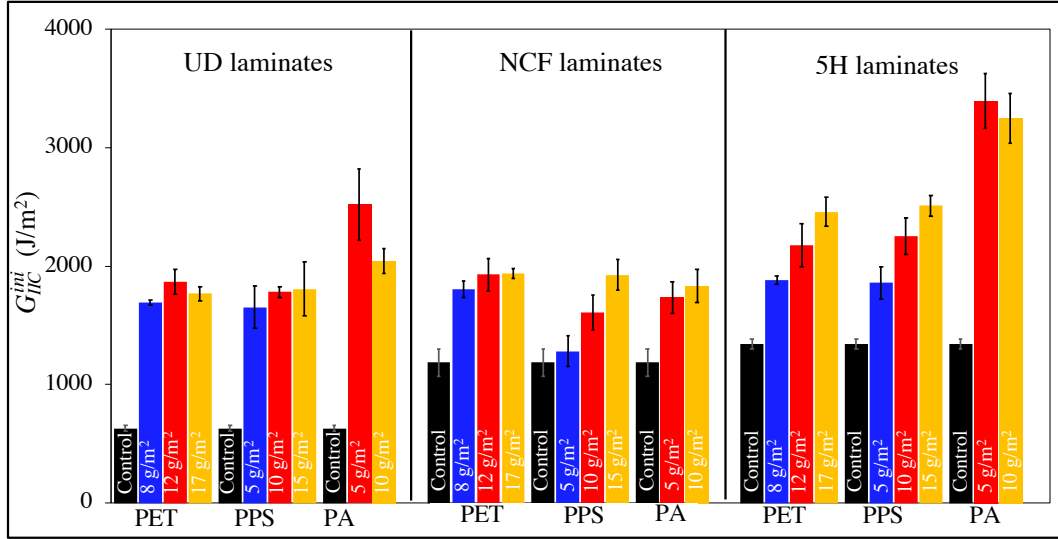
Table 4: G_{IIC} of the interleaved 5H composites. Values in brackets indicate percentage increase of G_{IIC} values over those of control specimens.

Specimens	G_{IIC}^{ini} (J/m ²)	$G_{IIC}^{plateau}$ (J/m ²)
5H/Control	1340±41	1731±85
5H/PET8	1881±37 (+40 %)	2875±208 (+66 %)
5H/PET12	2176±184 (+62 %)	3086±36 (+78 %)
5H/PET17	2459±124 (+84 %)	3435±150 (+98 %)
5H/PPS5	1859±136 (+39 %)	3066±175 (+77 %)
5H/PPS10	2250±154 (+68 %)	3144±119 (+82 %)
5H/PPS15	2510±87 (+87 %)	3248±99 (+88 %)
5H/PA10	3393±230 (+153 %)	3155±152 (+82 %)
5H/PA15	3249±210 (+142 %)	3728±197 (+115 %)

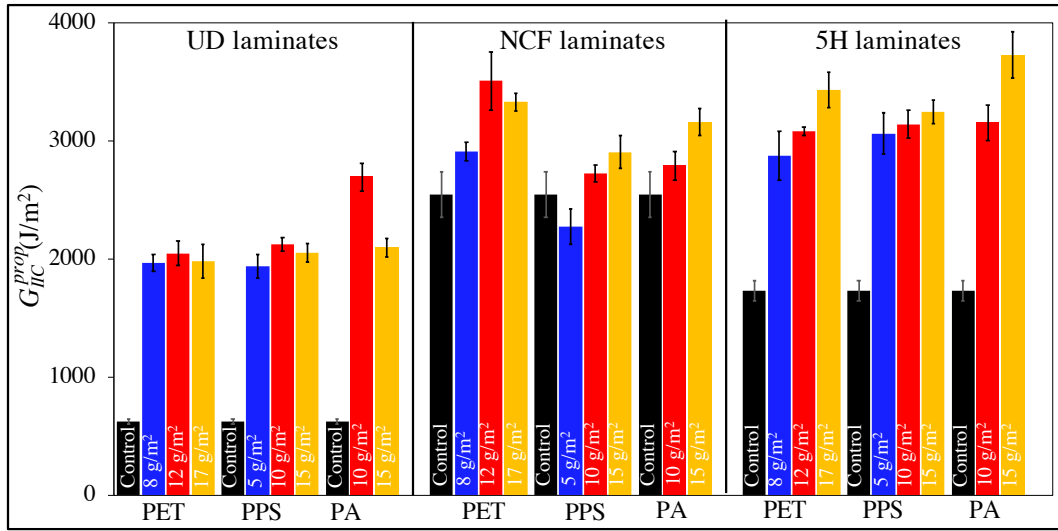
PA/epoxy layer and the carbon fibres) and carbon fibre delamination and bridging was the main fracture mechanism of the PA interleaved 5H laminates.

3.5. Fractography and Discussion

Figure 8 summarises the mode-II fracture energies of all the laminates interleaved by the thermoplastic veils. Significant improvements in the mode-II fracture performance were obtained for all the studied systems. In general, interlaying thermoplastic veils was more effective for toughening the UD laminates, which possessed a low original fracture toughness. An increase of between 163-300 % in G_{IIC}^{ini} was achieved for all the interleaved UD laminates, with an all-round maximum improvement of 300 % for the UD/PA10. The toughening efficiency of the thermoplastic veils was lower for the 5H laminates than the UD laminates. For example, the maximum increase in G_{IIC}^{ini} was observed to be 84 % (5H/PET17), 87 % (5H/PPS15) and 153 % (5H/PA10) for the 5H laminates interleaved by PET, PPS and PA veils, respectively. The lowest improvement in the fracture toughness was obtained for the NCF laminates, i.e. interlaying PET, PSS and PA veils increased G_{IIC}^{ini} of the NCF laminates by a maximum value of 64 % (NCF/PET17), 62 % (NCF/PPS15) and 55 % (NCF/PA15), re-



(a) G_{IIC}^{ini}



(b) G_{IIC}^{prop} ($G_{IIC}^{plateau}$ or G_{IIC}^{max})

Figure 8: A comparison of the G_{IIC}^{ini} and G_{IIC}^{prop} ($G_{IIC}^{plateau}$ or G_{IIC}^{max}) for all the laminates without and with veils.

spectively. Essentially the same toughening efficiency was observed for G_{IIC}^{prop} as that for G_{IIC}^{ini} . However, it should be noted that, all the interleaved NCF and 5H laminates possessed a higher absolute value of G_{IIC}^{prop} than the corresponding UD laminates, when they were interleaved with the same thermoplastic veil, as shown in Figure 8 (b).

Figure 9 presents representative SEM images of the fracture surfaces of the laminates without and with thermoplastic veils. It was found that only a relatively small number of delaminated and broken carbon fibres existed on the fracture surface of the UD/Control laminate, and all the carbon fibres were well-attached to the fracture surface of the NCF/Control laminate. This indicates limited to no carbon fibre bridging during the fracture of the UD and NCF controls. During the fracture process under a shear load, a high stress constraint was applied to the epoxy at the mid-plane by the surrounding carbon fibres. This generated the flake-like epoxy features on the fracture surfaces of all the control laminates. The presence of a large number of delaminated and broken carbon fibres on the fracture surface of the 5H control laminate demonstrated extensive carbon fibre bridging during the fracture process.

For the laminates interleaved with non-meltable PET and PPS veils, a layer of cracked epoxy resin containing a large number of thermoplastic fibres was observed on the fracture surfaces, see Figure 9 (d) (e) (g) (h) (j) and (k). This indicates that thermoplastic fibre bridging, associated with thermoplastic fibre pull-out, peel-off, plastic deformation and breakage, were the main toughening mechanisms of the PET and PPS veils for all the laminates. No thermoplastic fibres were observed on the fracture surfaces of the PA veil interleaved laminates (Figure 9 (f) (i) and (l)), and the addition of the meltable PA veils mainly improved the fracture toughness of the epoxy matrix and introduced a layer of tough PA resin at the mid-plane. This resulted in different toughening mechanisms of the PA veils for the UD, NCF and 5H laminates.

For the PA interleaved UD laminates, a large number of long cracks (aligned perpendicular to the fibre orientation direction), together with numerous grooves generated by the peel-off of the carbon fibres, appeared on the resin-rich side of the fracture surfaces, see Fig-

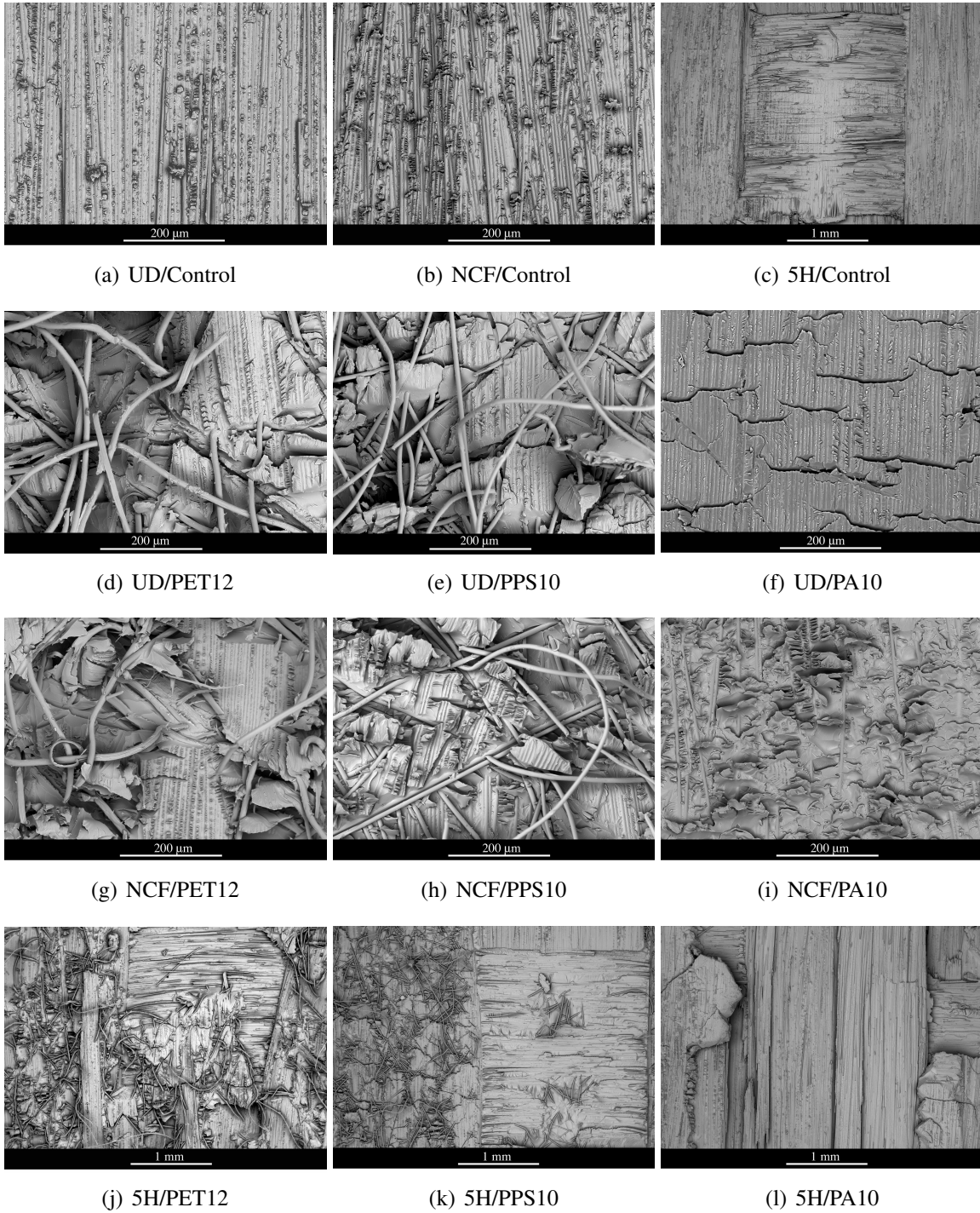


Figure 9: Representative SEM images of the fracture surfaces of the laminates without and with veils.

ure 9 (f). The formation of these cracks inside the PA toughened epoxy matrix contributed to additional fracture energy absorption. For the PA interleaved NCF laminates, apart from the introduced carbon fibre delamination (as shown in Figure 5), extensive plastic deformation of the PA resin was observed to be another toughening mechanism of the PA veils. This was evidenced by the presence of significant leaf-like features on the fracture surface of the NCF/PA10 laminate in Figure 9 (i). A comparison between Figures 9 (c) and (l) demonstrated that interlaying PA veils led to intensive delamination, bridging and breakage of the carbon fibres for the 5H laminates. This was analysed to be the main toughening mechanism of the PA veils for the 5H laminates.

To date, the majority of studies have focused on mode-I fracture behaviour of laminates interleaved with thermoplastic veils, with only a limited number of them considering mode-II fracture. Table 5 summarises the toughening performance of different thermoplastic veils for the mode-II fracture behaviour of carbon fibre/epoxy composites both in the literature and in this study. To the authors' knowledge, there have been no relevant studies on NCF laminates to date. Hence, this work demonstrated for the first time that interlaying thermoplastic veils can significantly improve the mode-II fracture behaviour of NCF laminates, which already possessed the highest fracture propagation energy when compared to the UD and 5H control laminates, as shown in Figure 8. Table 5 shows that the toughening efficiencies of interlaying thermoplastic veils into CFRPs were affected by the veil materials [14, 26, 28, 29], the areal density of the veils [20, 28, 33] and the architecture of the carbon fibre fabrics [20, 26, 28, 29]. This was observed in some cases of the current study. However, in this study, it was also found that the areal density of the veils had negligible effects for some interleaved CFRP systems (see Sections 3.2 and 3.4), as in which, interfacial failure between the thermoplastic veils and carbon fibres dominated the fracture process. From Table 5, it was observed that the increases of G_{IIC} upon interlaying thermoplastic veils varied significantly in different studies, with reductions being observed in a few cases (highlighted in bold). Besides the mentioned material and areal density of the veils and the architecture of the carbon fibre fabrics, another factor

Table 5: Toughening performance of different thermoplastic veils for UD and woven (plain, twill and satin weave) carbon fibre/epoxy composites.

Reference	Polymer (Scale)	Amount of veils	G_{IIC} (% increase)
UD laminates			
[20]	PA6,6 (Nano)	40,90 μ m thick	G_{IIC}^{ini} :+61,+62%
[28]	PA6,6 (Nano)	3,18 g/m ²	$G_{IIC}^{ini}/G_{IIC}^{prop}$:+46,+183%/+42,+188%
	PA6,9 (Nano)	3,18 g/m ²	$G_{IIC}^{ini}/G_{IIC}^{prop}$:+64,+183%/+67,+211%
[14]	PA6,6 (Nano)	4.5 g/m ²	G_{IIC}^{ini} :+69%
	PVB (Nano)	4.3 g/m ²	G_{IIC}^{ini} : -6%
	PCL (Nano)	4.2 g/m ²	G_{IIC}^{ini} :+7%
	PES (Nano)	3.6 g/m ²	G_{IIC}^{ini} :+20%
	PAI (Nano)	4.1 g/m ²	G_{IIC}^{ini} :+56%
[14]	PVB (Micro)	4.5 g/m ²	G_{IIC}^{ini} : -8%
[26, 29]	PE (Micro)	23 g/m ²	$G_{IIC}^{ini}/G_{IIC}^{prop}$:+57%/+44%
	PA (Micro)	21 g/m ²	$G_{IIC}^{ini}/G_{IIC}^{prop}$:+43%/+92%
This study	PET (Micro)	8,12,17 g/m ²	$G_{IIC}^{ini}/G_{IIC}^{prop}$:+168,+197,+181%/+214,+227,+216%
	PPS (Micro)	5,10,15 g/m ²	$G_{IIC}^{ini}/G_{IIC}^{prop}$:+163,+183,+187%/+209,+239,+227%
	PA (Micro)	10,15 g/m ²	$G_{IIC}^{ini}/G_{IIC}^{prop}$:+300,+224%/+330,+234%
NCF laminates	(No reference available)		
Woven laminates			
[28]	PA6,6 (Nano)	3,18 g/m ²	G_{IIC}^{ini} :+17,+100%
	PA6,9 (Nano)	3,18 g/m ²	G_{IIC}^{ini} :+35,+187%
[20]	PA6,6 (Nano)	40,90 μ m thick	$G_{IIC}^{ini}/G_{IIC}^{prop}$:+44,+99%/+34,+32%
[33]	Kevlar-49 (Micro)	5,10,15 g/m ²	$G_{IIC}^{ini}/G_{IIC}^{prop}$:+59,+51,+75%/+39,+33,+49%
[26, 29]	PE (Micro)	23 g/m ²	$G_{IIC}^{ini}/G_{IIC}^{prop}$:+38%/+82% (plain weave)
			$G_{IIC}^{ini}/G_{IIC}^{prop}$:+58%/ -46% (5H)
	PA (Micro)	21 g/m ²	$G_{IIC}^{ini}/G_{IIC}^{prop}$:+75%/+64% (plain weave)
			$G_{IIC}^{ini}/G_{IIC}^{prop}$:+68%/+0% (5H)
This study	PET (Micro)	8,12,17 g/m ²	$G_{IIC}^{ini}/G_{IIC}^{prop}$:+40,+62,+84%/+66,+78,+98%
	PPS (Micro)	5,10,15 g/m ²	$G_{IIC}^{ini}/G_{IIC}^{prop}$:+39,+68,+87%/+77,+82,+88%
	PA (Micro)	10,15 g/m ²	$G_{IIC}^{ini}/G_{IIC}^{prop}$:+153,+142%/+82,+115%

* PVB: Polyvinyl butyral; PCL: Polycaprolactone; PES: Polyethersulfone; PAI: Polyamide-imides; PE: Polyethylene.

that can significantly affect the toughening performance of the veils is the adhesion (compatibility) between the thermoplastic veils and the epoxy matrix [34]. Nevertheless, there is still a lack of research on this topic, even for the mostly studied mode-I fracture. It is worth noting that the compatibility between thermoplastics and epoxy is typically poor due to the inherently low reactivity, small surface energies and weak polarities of thermoplastics [35]. Our previous work [36] demonstrated that doping a small amount of multi-walled carbon nanotubes (MWCNTs) onto the thermoplastic veils could improve the adhesion between the thermoplastic fibres and the epoxy matrix, and subsequently enhance the toughening performance of the veils. In contrast, the presence of graphene nano-platelet (GNPs) on the thermoplastic veils reduced the thermoplastic fibre/epoxy adhesion and resulted in notable drops in the fracture energies of the interleaved laminates. It was also proven that there is an optimal thermoplastic veil/epoxy adhesion for toughening performance, i.e. thermoplastic fibre bridging vanished as the veil/adhesion increased to a certain level that was sufficient to prevent the debonding of thermoplastic fibres from the epoxy [36, 37]. In this case, the majority of the thermoplastic fibres could not be pulled out but were directly broken during the crack propagation, that led to detrimental effects on the toughening behaviour. The same trend was also observed by Wang et al. [38]. A comparison between the results of the current work and the other literature in Table 5 provided some evidence showing that the curing process of the laminates might be critical for the toughening performance of the veils, which can subsequently affect the compatibility between the thermoplastic veils and the epoxy matrix. For example, the meltable PA veils used in this work were superior for toughening the CFRPs, i.e. the maximum increase in G_{IIC}^{ini} was measured to be +300 % and +153 % for the UD and woven laminates upon interlaying the PA veils, respectively. This was because the laminate curing temperature of 180 °C was high enough to melt the PA veils and hence achieve relatively good compatibility between the epoxy matrix and the PA veils. For the non-melted PET and PPS veils, the toughening levels of thermoplastic veils in the literature [28] and in this study were outstanding, as shown in Table 5. The commonality between these two stud-

ies was that the laminates were cured under both relatively high pressure (0.5 or 0.6 MPa) and high temperature (with a section of the curing process at 180 °C), that could benefit the interaction/compatibility between the thermoplastic veils and the epoxy matrix during the curing process. The effects of the laminate curing process on the toughening levels of thermoplastic veils were considered by Wang et al. [38], who used carbon black (CB) doped thermoplastic veils as interlayers of CFRPs and applied various post-curing procedures with different pressures and temperatures. The results demonstrated significant effects of the post curing temperature and pressure on the fracture behaviour of the interleaved laminates. A SEM analysis revealed that this was due to the different compatibility between the thermoplastic veils and the epoxy, i.e. a higher temperature or pressure resulted in better thermoplastic fibre/epoxy adhesion [38]. Overall, the observations in the current work and in the literature [36–38] indicate that the adhesion between the epoxy matrix and the thermoplastic veils is a critical factor on the toughening performance of thermoplastic veils. Nevertheless, to conclusively understand the effects of thermoplastic veil/epoxy adhesion on the toughening performance of the veils, additional studies on the interleaved CFRP systems with tailored thermoplastic veil/epoxy adhesion values, but no additional modifiers are still required.

4. Conclusions

Thermoplastic veils based on Polyethylene terephthalate (PET), Polyphenylene sulfide (PPS) and Polyamide-12 (PA) polymers with different areal densities were used to enhance the interlaminar fracture toughness of unidirectional (UD), non-crimp fabric (NCF) and 5-Harness satin weave (5H) carbon fibre laminates. Significant improvements in the mode-II fracture toughness were observed for all the interleaved laminates. Interlaying thermoplastic veils toughened the UD laminates most efficiently, followed by the 5H laminates, and then the NCF laminates. For instance, an increase of between 163-300 % in G_{IIC}^{ini} was achieved for all the interleaved UD laminates, with an all-round maximum improvement of 300 % observed for the UD laminates interleaved by a 10 g/m² PA veil. The all-round maximum

improvements in G_{IIC}^{ini} for the 5H and NCF laminates were 153 % (5H/PA10) and 64 % (NCF/PET17), respectively. Thermoplastic fibre bridging, accompanied by the pull-out, peel-off, plastic deformation and breakage of the thermoplastic fibres, was determined to be the main toughening mechanism of the non-meltable PET and PPS veils for all the laminates. Interlaying meltable PA veils mainly increased the fracture toughness of the epoxy matrix at the mid-plane. The different toughening mechanisms of the veils, together with the different fracture mechanisms of the UD, NCF and 5H laminates, resulted in significantly different fracture performance and mechanisms of the interleaved laminates.

Acknowledgements

The authors gratefully acknowledge the financial support of the Irish Composites Centre. We would also like to thank Bombardier Aerospace (UK) and Technical Fibre Products (UK) for supplying the carbon fibre fabrics and thermoplastic veils employed in this study. Dong Quan received funding from the European Union's Horizon 2020 research and innovation programme under the Marie Skłodowska-Curie grant agreement No. 842467.

References

- [1] S. Sprenger, M. H. Kothmann, V. Altstaedt, Carbon fiber-reinforced composites using an epoxy resin matrix modified with reactive liquid rubber and silica nanoparticles, *Composites Science and Technology* 105 (2014) 86 – 95. doi:10.1016/j.compscitech.2014.10.003.
- [2] D. Quan, J. L. Urdaniz, A. Ivankovic, Enhancing mode-I and mode-II fracture toughness of epoxy and carbon fibre reinforced epoxy composites using multi-walled carbon nanotubes, *Materials & Design* 143 (2018) 81 – 92. doi:10.1016/j.matdes.2018.01.051.

- [3] Y. Xu, S. V. Hoa, Mechanical properties of carbon fiber reinforced epoxy/clay nanocomposites, *Composites Science and Technology* 68 (3) (2008) 854 – 861. doi:10.1016/j.compscitech.2007.08.013.
- [4] G. Stegenschuster, K. Pingkarawat, B. Wendland, A. Mouritz, Experimental determination of the mode-I delamination fracture and fatigue properties of thin 3D woven composites, *Composites Part A: Applied Science and Manufacturing* 84 (2016) 308 – 315. doi:10.1016/j.compositesa.2016.02.008.
- [5] B. M'membe, M. Yasaei, S. R. Hallett, I. K. Partridge, Effective use of metallic Z-pins for composites' through-thickness reinforcement, *Composites Science and Technology* 175 (2019) 77 – 84. doi:10.1016/j.compscitech.2019.02.024.
- [6] R. Velmurugan, S. Solaimurugan, Improvements in Mode-I interlaminar fracture toughness and in-plane mechanical properties of stitched glass/polyester composites, *Composites Science and Technology* 67 (1) (2007) 61 – 69. doi:10.1016/j.compscitech.2006.03.032.
- [7] H. Zhou, X. Du, H.-Y. Liu, H. Zhou, Y. Zhang, Y.-W. Mai, Delamination toughening of carbon fiber/epoxy laminates by hierarchical carbon nanotube-short carbon fiber interleaves, *Composites Science and Technology* 140 (2017) 46 – 53. doi:10.1016/j.compscitech.2016.12.018.
- [8] H. Ning, J. Li, N. Hu, C. Yan, Y. Liu, L. Wu, F. Liu, J. Zhang, Interlaminar mechanical properties of carbon fiber reinforced plastic laminates modified with graphene oxide interleaf, *Carbon* 91 (2015) 224 – 233. doi:10.1016/j.carbon.2015.04.054.
- [9] D. Quan, S. Flynn, M. Artuso, N. Murphy, C. Rouge, A. Ivankovic, Interlaminar fracture toughness of CFRPs interleaved with stainless steel fibres, *Composite Structures* 210 (2019) 49 – 56. doi:10.1016/j.compstruct.2018.11.016.

- [10] M. Hojo, S. Matsuda, M. Tanaka, S. Ochiai, A. Murakami, Mode I delamination fatigue properties of interlayer-toughened CF/epoxy laminates, *Composites Science and Technology* 66 (5) (2006) 665 – 675. doi:/10.1016/j.compscitech.2005.07.038.
- [11] R. Palazzetti, A. Zucchelli, C. Gualandi, M. Focarete, L. Donati, G. Minak, S. Ramakrishna, Influence of electrospun nylon 6,6 nanofibrous mats on the interlaminar properties of Gr-epoxy composite laminates, *Composite Structures* 94 (2) (2012) 571 – 579. doi:10.1016/j.compstruct.2011.08.019.
- [12] B. Behera, B. Dash, Mechanical behavior of 3D woven composites, *Materials & Design* 67 (2015) 261 – 271. doi:10.1016/j.matdes.2014.11.020.
- [13] J. Hoffmann, G. Scharr, Compression properties of composite laminates reinforced with rectangular z-pins, *Composites Science and Technology* 167 (2018) 463 – 469. doi:10.1016/j.compscitech.2018.08.042.
- [14] G. W. Beckermann, K. L. Pickering, Mode I and Mode II interlaminar fracture toughness of composite laminates interleaved with electrospun nanofibre veils, *Composites Part A: Applied Science and Manufacturing* 72 (2015) 11 – 21. doi:10.1016/j.compositesa.2015.01.028.
- [15] B. Beylergil, M. Tanoglu, E. Aktas, Enhancement of interlaminar fracture toughness of carbon fiber/epoxy composites using polyamide-6,6 electrospun nanofibers, *Journal of Applied Polymer Science* 134 (35) (2017) 45244. doi:10.1002/app.45244.
- [16] B. Beylergil, M. Tanoglu, E. Aktas, Effect of polyamide-6,6 (PA 66) nonwoven veils on the mechanical performance of carbon fiber/epoxy composites, *Composite Structures* 194 (2018) 21 – 35. doi:10.1016/j.compstruct.2018.03.097.

- [17] B. Beylergil, M. Tanoglu, E. Aktas, Mode-I fracture toughness of carbon fiber/epoxy composites interleaved by aramid nonwoven veils, *Steel and Composite Structures* 31 (2) (2019) 113–123. doi:10.12989/scs.2019.31.2.113.
- [18] R. Palazzetti, A. Zucchelli, I. Trendafilova, The self-reinforcing effect of Nylon 6,6 nano-fibres on CFRP laminates subjected to low velocity impact, *Composite Structures* 106 (2013) 661 – 671. doi:10.1016/j.compstruct.2013.07.021.
- [19] H. Saghafi, A. Zucchelli, R. Palazzetti, G. Minak, The effect of interleaved composite nanofibrous mats on delamination behavior of polymeric composite materials, *Composite Structures* 109 (2014) 41 – 47. doi:10.1016/j.compstruct.2013.10.039.
- [20] T. Brugo, R. Palazzetti, The effect of thickness of Nylon 6,6 nanofibrous mat on Modes I-II fracture mechanics of UD and woven composite laminates, *Composite Structures* 154 (2016) 172 – 178. doi:10.1016/j.compstruct.2016.07.034.
- [21] R. Palazzetti, A. Zucchelli, Electrospun nanofibers as reinforcement for composite laminates materials-A review, *Composite Structures* 182 (2017) 711 – 727. doi:10.1016/j.compstruct.2017.09.021.
- [22] D. W. Wong, L. Lin, P. T. McGrail, T. Peijs, P. J. Hogg, Improved fracture toughness of carbon fibre/epoxy composite laminates using dissolvable thermoplastic fibres, *Composites Part A: Applied Science and Manufacturing* 41 (6) (2010) 759 – 767. doi:10.1016/j.compositesa.2010.02.008.
- [23] L. M. K. Molnar, E. Kostakova, The effect of needleless electrospun nanofibrous interleaves on mechanical properties of carbon fabrics/epoxy laminates, *eXPRESS Polymer Letters* 8 (1) (2014) 62–72. doi:10.3144/expresspolymlett.2014.8.

- [24] B. Beylergil, M. Tanoglu, E. Aktas, Modification of carbon fibre/epoxy composites by polyvinyl alcohol (PVA) based electrospun nanofibres, *Advanced Composites Letters* 25 (3) (2016) 69–76. doi:10.1177/096369351602500303.
- [25] J. Zhang, T. Yang, T. Lin, C. H. Wang, Phase morphology of nanofibre interlayers: Critical factor for toughening carbon/epoxy composites, *Composites Science and Technology* 72 (2) (2012) 256 – 262. doi:10.1016/j.compscitech.2011.11.010.
- [26] M. Kuwata, P. Hogg, Interlaminar toughness of interleaved CFRP using non-woven veils: Part 1. Mode-I testing, *Composites Part A: Applied Science and Manufacturing* 42 (10) (2011) 1551 – 1559. doi:10.1016/j.compositesa.2011.07.016.
- [27] G. W. Beckermann, Nanofiber interleaving veils for improving the performance of composite laminates, *Reinforced Plastics* 61 (5) (2017) 289 – 293. doi:10.1016/j.repl.2017.03.006.
- [28] L. Daelemans, S. van der Heijden, I. D. Baere, H. Rahier, W. V. Paepegem, K. D. Clerck, Nanofibre bridging as a toughening mechanism in carbon/epoxy composite laminates interleaved with electrospun polyamide nanofibrous veils, *Composites Science and Technology* 117 (2015) 244 – 256. doi:10.1016/j.compscitech.2015.06.021.
- [29] M. Kuwata, P. Hogg, Interlaminar toughness of interleaved CFRP using non-woven veils: Part 2. Mode-II testing, *Composites Part A: Applied Science and Manufacturing* 42 (10) (2011) 1560 – 1570. doi:10.1016/j.compositesa.2011.07.017.
- [30] N. Zheng, Y. Huang, H.-Y. Liu, J. Gao, Y.-W. Mai, Improvement of interlaminar fracture toughness in carbon fiber/epoxy composites with carbon nanotubes/polysulfone interleaves, *Composites Science and Technology* 140 (2017) 8 – 15. doi:10.1016/j.compscitech.2016.12.017.

- [31] D. Quan, F. Bologna, G. Scarselli, A. Ivankovic, N. Murphy, Interlaminar fracture toughness of aerospace-grade carbon fibre reinforced plastics interleaved with thermoplastic veils, *Composites Part A: Applied Science and Manufacturing* 128 (2020) 105642. doi:10.1016/j.compositesa.2019.105642.
- [32] ISO 15114:2014, Fibre-reinforced plastic composites Determination of mode II fracture resistance for unidirectionally reinforced materials using the calibrated end-loaded split (C-ELS) test and an effective crack length approach (2014).
- [33] S. Yadav, V. Kumar, S. K. Verma, Fracture toughness behaviour of carbon fibre epoxy composite with kevlar reinforced interleave, *Materials Science and Engineering: B* 132 (1) (2006) 108 – 112. doi:10.1016/j.mseb.2006.02.026.
- [34] K. Bilge, M. Papila, 10 - interlayer toughening mechanisms of composite materials, in: Q. Qin, J. Ye (Eds.), *Toughening Mechanisms in Composite Materials*, Woodhead Publishing Series in Composites Science and Engineering, Woodhead Publishing, 2015, pp. 263 – 294. doi:10.1016/B978-1-78242-279-2.00010-X.
- [35] S. Deng, L. Djukic, R. Paton, L. Ye, Thermoplastic/epoxy interactions and their potential applications in joining composite structures - A review, *Composites Part A: Applied Science and Manufacturing* 68 (2015) 121 – 132. doi:10.1016/j.compositesa.2014.09.027.
- [36] D. Quan, C. Mischo, L. Binsfeld, A. Ivankovic, N. Murphy, Fracture behaviour of carbon fibre/epoxy composites interleaved by MWCNT- and graphene nanoplatelet-doped thermoplastic veils, *Composite Structures* (2019) 111767doi:10.1016/j.compstruct.2019.111767.
- [37] D. Quan, C. Mischo, X. Li, G. Scarselli, A. Ivankovic, N. Murphy, Improving the electrical conductivity and fracture toughness of carbon fibre/epoxy composites by inter-

leaving MWCNT-doped thermoplastic veils, *Composites Science and Technology* 182 (2019) 107775. doi:10.1016/j.compscitech.2019.107775.

- [38] J. Wang, C. Ma, G. Chen, P. Dai, Interlaminar fracture toughness and conductivity of carbon fiber/epoxy resin composite laminate modified by carbon black-loaded polypropylene non-woven fabric interleaves, *Composite Structures* (2019) 111649doi:10.1016/j.compstruct.2019.111649.